

# Pattern Formation on the Edge of Chaos: CO Oxidation on Pt(110) under Global Delayed Feedback

Matthias Bertram, Michael Pollmann, Harm H. Rotermund, Alexander S. Mikhailov, and Gerhard Ertl  
*Fritz-Haber-Institut der Max-Planck-Gesellschaft, Faradayweg 4-6, D-14195 Berlin, Germany*  
(November 15, 2018)

Experiments with catalytic CO oxidation on Pt(110) show that chemical turbulence in this system can be suppressed by application of appropriate global delayed feedbacks. Different spatiotemporal patterns, seen near a transition from turbulence to uniform oscillations, are investigated. Using a method based on the Hilbert transform, spatial distributions of local phase and amplitude in such patterns are reconstructed from the experimental data. The observed phenomena are reproduced in simulations using a theoretical model of the reaction.

82.40.Np, 82.40.Bj, 05.45.Gg

Control of chaos is one of the central problems in nonlinear dynamics. In contrast to existing exact methods [1], a heuristic approach based on the introduction of delayed feedbacks does not require extensive real-time computations [2]. For extended systems, where spatially resolved access is difficult, global delayed feedbacks can be employed. In such methods, information continuously gathered from all elements is summed up and used to generate a signal which is applied back to control a common system parameter. Global feedbacks can be employed to stabilize otherwise unstable trajectories, but also as a tool to produce new spatiotemporal patterns. Action of global feedbacks on chaotic extended systems has been experimentally and theoretically investigated for lasers [3,4], gas discharges [5], semiconductors [6], populations of electrochemical oscillators [7], and surface chemical reactions [8]; it was also discussed in a general context of the complex Ginzburg-Landau equation [9,10]. Furthermore, various forms of global feedback have been successfully applied to control pattern formation in non-chaotic excitable [11–13] and oscillatory [14–17] chemical systems.

Nonequilibrium systems on the edge of chaos are capable to generate a broad variety of complex patterns. To bring a system to a boundary between deterministic and chaotic dynamics, its parameters may be appropriately chosen or external forcing may be introduced. However, a practical implementation of such a predefined control meets serious difficulties because a system at the edge of chaos is sensitive even to small parameter variations. An alternative is provided by using a global delayed feedback. The advantage of this method is that an acting force is generated by the system itself and therefore automatically adjusts to the variations of experimental con-

ditions.

In this Letter, we apply a global delayed feedback to investigate spatiotemporal pattern formation near a transition to chaos in an oscillatory surface chemical reaction of catalytic CO oxidation on Pt(110). Chemical turbulence in this reaction has previously been observed [18]. Theoretical analysis has shown the possibility for its existence both under excitable [19] and oscillatory [20] conditions. Experiments on suppression of chaos by global delayed feedbacks in catalytic CO oxidation have recently been reported [8]. In the present study, the attention is focused on the characterization of complex spatiotemporal patterns resulting from the application of such global feedbacks. A variety of spatiotemporal structures exhibited upon variation of the feedback intensity and delay time is investigated.

The catalytic oxidation of carbon monoxide on a platinum(110) single crystal surface follows a relatively simple mechanism [21]. Molecules of CO and oxygen from the gas phase adsorb on the catalytic surface before the reaction. Adsorbed CO molecules diffuse and react with immobile adsorbed oxygen atoms to produce carbon dioxide that immediately leaves the surface. Temporal oscillations of the reaction rate are due to an adsorbate-driven surface reconstruction in the top substrate layer. The interplay between reaction and diffusion leads to the development of spatiotemporal patterns including rotating spiral waves, target patterns, and turbulence [18].

For the visualization of such patterns, photoemission electron microscopy (PEEM) is used [22]. This method displays the local work function across a surface area of about  $500\ \mu\text{m}$  in diameter. In our experiments, PEEM images were recorded at a rate of 25 per second. The pressure gauges for  $\text{O}_2$  and CO allowed controlled dosing of reactants into the reaction chamber. Global delayed feedback was introduced by making the instantaneous dosing rate of CO molecules dependent on the properties of imaged concentration patterns. To generate the control signal  $I(t)$ , the local PEEM intensity [23] was averaged over the entire observation window. The dosing rate of CO was varied according to this signal with a delay  $\tau_d$ . The variation of the CO partial pressure  $p_{\text{CO}}$  in the chamber followed the temporal modulation of the dosing rate with an additional delay determined by the residence time of gases in the pumped chamber. Thus, a controlled feedback was introduced, such that  $p_{\text{CO}}(t) = p_0 + \mu [I(t - \tau) - I_0]$ , where  $\tau$  is the effec-

tive time delay, the parameter  $\mu$  specifies the feedback intensity, and  $p_0$  and  $I_0$  are the partial CO pressure and the mean base level of the integral PEEM intensity in absence of feedback. Gas-phase coupling also leads to intrinsic variations of partial pressures [24], but these were significantly smaller than the artificially introduced variation and could be neglected here.

In the beginning of each experiment, temperature and partial pressures were chosen in such a way that the reaction was oscillatory and, furthermore, the unforced pattern represented a state of turbulence where fragments of rotating spiral waves spontaneously developed and died out at different locations. After some time the feedback was switched on and its parameters could be varied. In experiments with a systematic variation of the parameters  $\mu$  and  $\tau$ , we have observed that such turbulence could be suppressed and replaced by stable uniform oscillations for any delay time (delays up to  $\tau = 10$  s were probed) if the feedback intensity  $\mu$  was sufficiently high (up to  $5 \times 10^{-5}$  mbar, corresponding to CO partial pressure variations of about 20%). Usually, the synchronization threshold was significantly lower (about 5% variations in  $p_{\text{CO}}$ ). The period of uniform oscillations was affected by the feedback and varied approximately between 3 s and 10 s, increasing for longer delays and decreasing for stronger feedbacks.

By fixing the feedback intensity below the transition to uniform oscillations, various spatiotemporal patterns could be observed. PEEM images of several typical patterns are displayed in the top row in Fig. 1. Dark (blue) areas are predominantly O covered; bright (red) regions are mainly CO covered. In absence of feedback, spiral-wave turbulence is observed [Fig. 1(a)]. As  $\mu$  is increased, the feedback becomes effective and global oscillations set on. Turbulent spiral waves are then replaced by the states of intermittent turbulence characterized by localized ring-shaped structures or localized spiral-wave fragments on a uniformly oscillating background [Figs. 1(b) and 1(c)]. Such objects repeatedly reproduce until many of them are found, and again annihilate such that only a few survive. Intermittent turbulence is found independent of the delay time. In addition, for delays in the interval  $0.5 \text{ s} < \tau < 1.0 \text{ s}$ , two-phase clusters [Fig. 1(d)], irregular arrays of cells [Fig. 1(e)], or oscillatory standing waves [Fig. 1(f)] may develop close to the transition to uniform oscillations.

To characterize the observed patterns, we have employed a variant of the analytic signal approach [25,26]. This method has allowed us to transform sequences of typically 250 experimental PEEM images into the time-dependent spatial distribution of phase and amplitude variables. For the local PEEM intensity  $s(\mathbf{x}, t)$  at an observation point  $\mathbf{x}$ , its Hilbert transform  $\tilde{s}(\mathbf{x}, t) = \pi^{-1} \int_{-\infty}^{\infty} (t - t')^{-1} s(\mathbf{x}, t') dt'$  was computed (this could be easily realized by determining the Fourier transform of

$s$ , shifting it by  $\pi/2$ , and performing the reverse Fourier transform). This was repeatedly done for all pixel points  $\mathbf{x}$  in an  $100 \times 100$  array covering the respective pattern. Using  $s(\mathbf{x}, t)$  and its Hilbert transform  $\tilde{s}(\mathbf{x}, t)$ , a complex variable  $\zeta(\mathbf{x}, t) = s(\mathbf{x}, t) + i \tilde{s}(\mathbf{x}, t)$  was defined. The local oscillation phase  $\phi(\mathbf{x}, t)$  and amplitude  $R(\mathbf{x}, t)$  were computed as  $\phi = \arg \zeta$  and  $R = \rho / \rho_{\text{ref}}(\phi)$  where  $\rho = |\zeta|$  and the normalization to  $\rho_{\text{ref}}(\phi)$  was introduced to approximately compensate for deviations from harmonicity in the observed oscillations. To obtain  $\rho_{\text{ref}}(\phi)$  the statistical distribution of  $\zeta$  for all  $100 \times 100$  pixels and at all 250 time moments was plotted into the complex plane, as illustrated in Fig. 1(g) for a set of spatiotemporal data representing a pattern of spiral-wave turbulence. We determined  $\rho_{\text{ref}}(\phi)$  as a statistical average of  $\rho = |\zeta|$  inside each of 200 equidistant narrow intervals of the polar angle  $\phi$ . Note that the closed curve  $\rho = \rho_{\text{ref}}(\phi)$  in the complex plane can be viewed as representing a reference orbit of the system deduced from the experimental data.

By applying this transformation separately to each of the PEEM patterns shown in Fig. 1, spatial distributions of the phase  $\phi$  and amplitude  $R$  in each pattern were constructed. Additionally, Fig. 1 shows a phase portrait of each pattern, obtained by displaying the amplitudes and phases for all resolving pixels in polar coordinates. The phase  $\phi$  of a point is represented by the polar angle and the amplitude  $R$  is the distance to the coordinate origin.

In spiral-wave turbulence [Fig. 1(a)], the fluctuations of amplitude and phase are strong, as indicated by the broad-band structure in the phase portrait, and the amplitude drops down in the spiral cores. For intermittent turbulence [Figs. 1(b) and 1(c)], the amplitude and the phase are almost constant in the main part of the medium where uniform oscillations take place. The amplitude is significantly decreased in the ring-shaped objects [Fig. 1(b)] and small localized spirals [Fig. 1(c)], so that they represent extended amplitude defects. The phase portraits of the intermittent turbulence show a spot corresponding to the uniform state of the medium and a tail corresponding to the amplitude defects. In a cluster pattern [Fig. 1(d)] the medium breaks into two phase states seen as two spots in the phase portrait. The amplitudes in the two clusters differ because local oscillations exhibit period-doubling [8]. The “bridge” in the phase portrait connecting the two spots corresponds to the interfaces between the cluster domains; note that the phase varies smoothly and the amplitude is not significantly reduced at the interface for such cluster patterns. In cellular structures [Fig. 1(e)], small phase modulations are observed, while the amplitude remains approximately constant. In standing waves [Fig. 1(f)], both the phase and the amplitude are periodically modulated.

The effects of global delayed feedback on chemical turbulence have been theoretically investigated using a model [27,24] of the catalytic CO oxidation on Pt(110):

$$\dot{u} = k_1 s_{\text{CO}} p_{\text{CO}} (1 - u^3) - k_2 u - k_3 u v + D \nabla^2 u, \quad (1)$$

$$\dot{v} = k_4 p_{\text{O}_2} [s_{\text{O},1x1} w + s_{\text{O},1x2} (1 - w)] (1 - u - v)^2 - k_3 u v, \quad (2)$$

$$\dot{w} = k_5 [1 + \exp((u_0 - u) / \delta u)]^{-1} - k_5 w. \quad (3)$$

Here, the variables  $u$ ,  $v$ , and  $w$  represent the CO and oxygen surface coverage and the local fraction of the surface area in the nonreconstructed state. To account for global delayed feedback, we assume that the CO partial pressure  $p_{\text{CO}}$  in Eq. (1) is not constant but varies as  $p_{\text{CO}}(t) = p_0 - \mu [u_{\text{av}}(t - \tau) - u_{\text{ref}}]$ , where  $u_{\text{av}}(t)$  is the spatial average of the CO coverage  $u(\mathbf{x}, t)$  at time  $t$ , the parameter  $\mu$  specifies the feedback intensity,  $\tau$  is the delay time,  $p_0$  is the base level of the partial CO pressure, and  $u_{\text{ref}}$  is the CO coverage in the unstable steady state in absence of feedback. The parameters of the model are chosen in such a way that uniform oscillations are unstable and amplitude turbulence spontaneously develops without feedback. No-flux boundary conditions were imposed. Numerical integration of the model equations yields time-dependent concentration patterns which were further processed to reconstruct oscillation amplitudes and phases. Because the simulations already provide two variables, the Hilbert transformation is not necessary here and a simpler procedure described in Ref. [16] was instead used.

Figure 2 displays examples of different typical two-dimensional patterns. The unforced turbulence [Fig. 2(a)] is characterized by strong amplitude and phase fluctuations. Stabilization of uniform oscillations by sufficiently strong feedbacks is found in the model for the delays  $\tau > 0.1\text{s}$ . The intermittent turbulence [Fig. 2(b)] is characterized by irregular cascades of "bubbles" developing into ring-shaped structures on the background of uniform oscillations. The amplitude is strongly decreased inside such localized objects. Stationary two-phase clusters [Fig. 2(c)] are observed under further increase of the feedback intensity in narrow intervals of the delay time  $\tau$ . The total area occupied by each of the two cluster domains is equal. Local oscillations are period-doubled inside the cluster domains. At their interface, the oscillation amplitude does not vanish, but local oscillations are not period-doubled in the middle of the interface. When  $\tau$  is chosen outside of the cluster intervals (and  $\tau > 0.1\text{s}$ ), intermittent turbulence is directly replaced by uniform oscillations upon an increase of  $\mu$ . A hysteresis effect is found in the model: when the feedback intensity  $\mu$  is gradually decreased starting from uniform oscillations, turbulence may set on only at significantly lower values of  $\mu$ . Patterns representing regular and irregular oscillatory arrays of cells [Figs. 2(d) and 2(e)] are then observed in certain intervals of the delay time. These states are stable with respect to small perturbations, but transform into amplitude turbulence if stronger perturbations are applied. Both the phase and the amplitude

are modulated in such structures, though the amplitude variations are weak.

Thus, our simulations using a realistic model of the CO oxidation reaction successfully reproduce the principal kinds of patterns seen in the experiments. Remarkably, the results of our investigations agree with previous studies [9,10] of global feedbacks in oscillatory turbulent systems in the framework of the complex Ginzburg-Landau equation where clusters, oscillatory cellular arrays, and intermittent turbulence characterized by cascades of ring-shaped amplitude defects were also found. This indicates that the observed effects of pattern formation near the edge of chaos may be typical for a broad class of reaction-diffusion systems. To characterize the patterns, we have processed the data to approximately reconstruct amplitude and phase variables. This representation allows to directly compare the properties of patterns in systems of different origins and provides a link to the general studies of turbulence in oscillatory reaction-diffusion systems [28,29].

Financial support of the Deutsche Forschungsgemeinschaft under SFB 555 "Complex nonlinear processes" is acknowledged.

- 
- [1] E. Ott, C. Grebogi, and J. A. Yorke, *Phys. Rev. Lett.* **64**, 1196 (1990).
  - [2] K. Pyragas, *Phys. Lett. A* **170**, 421 (1992).
  - [3] M. E. Bleich, D. Hochheiser, J. V. Moloney, and J. E. S. Socolar, *Phys. Rev. E* **55**, 2119 (1997).
  - [4] M. Münkkel, F. Kaiser, and O. Hess, *Phys. Rev. E* **56**, 3868 (1997).
  - [5] T. Pierre, G. Bonhomme, and A. Atipo, *Phys. Rev. Lett.* **76**, 2290 (1996).
  - [6] G. Franceschini, S. Bose, and E. Schöll, *Phys. Rev. E* **60**, 5426 (1999).
  - [7] W. Wang, I. Z. Kiss, and J. L. Hudson, *Phys. Rev. Lett.* **86**, 4954 (2001).
  - [8] M. Kim *et al.*, *Science* **292**, 1357 (2001).
  - [9] D. Battogtokh and A. S. Mikhailov, *Physica D* **90**, 84 (1996).
  - [10] D. Battogtokh, A. Preusser, and A. S. Mikhailov, *Physica D* **106**, 327 (1997).
  - [11] K. Krischer and A. Mikhailov, *Phys. Rev. Lett.* **73**, 3165 (1994).
  - [12] O.-U. Kheowan *et al.*, *Phys. Rev. E* **64**, 035201(R) (2001).
  - [13] E. Mihaliuk, T. Sakurai, F. Chirila, and K. Showalter, *Discuss. Faraday Soc.* (to be published).
  - [14] V. K. Vanag *et al.*, *Nature* **406**, 389 (2000).
  - [15] L. Yang, M. Dolnik, A. M. Zhabotinsky, and I. R. Epstein, *Phys. Rev. E* **62**, 6414 (2000).
  - [16] M. Bertram and A. S. Mikhailov, *Phys. Rev. E* **63**, 066102 (2001).

- [17] M. Pollmann, M. Bertram, and H. H. Rotermund, Chem. Phys. Lett. **346**, 123 (2001).
- [18] S. Jakubith *et al.*, Phys. Rev. Lett. **65**, 3013 (1990).
- [19] M. Bär and M. Eiswirth, Phys. Rev. E **48**, R1635 (1993).
- [20] M. Falcke and H. Engel, J. Chem. Phys. **101**, 6255 (1994).
- [21] R. Imbihl and G. Ertl, Chem. Rev. **95**, 697 (1995).
- [22] H. H. Rotermund, Surf. Sci. Rep. **29**, 265 (1997).
- [23] The PEEM intensity is defined here in such a way that darker image areas have higher intensity.
- [24] A. von Oertzen, H. H. Rotermund, A. S. Mikhailov, and G. Ertl, J. Phys. Chem. B **104**, 3155 (2000).
- [25] P. Panter, *Modulation, Noise, and Spectral Analysis* (McGraw-Hill, New York, 1965).
- [26] M. Rosenblum and J. Kurths, in *Nonlinear Analysis of Physiological Data*, edited by H. Kantz, J. Kurths, and G. Mayer-Kress (Springer, Berlin, 1998), p. 91.
- [27] K. Krischer, M. Eiswirth, and G. Ertl, J. Chem. Phys. **96**, 9161 (1992).
- [28] Y. Kuramoto, *Chemical Oscillations, Waves, and Turbulence* (Springer, Berlin, 1984).
- [29] H. Chaté and P. Manneville, Physica A **224**, 348 (1996).

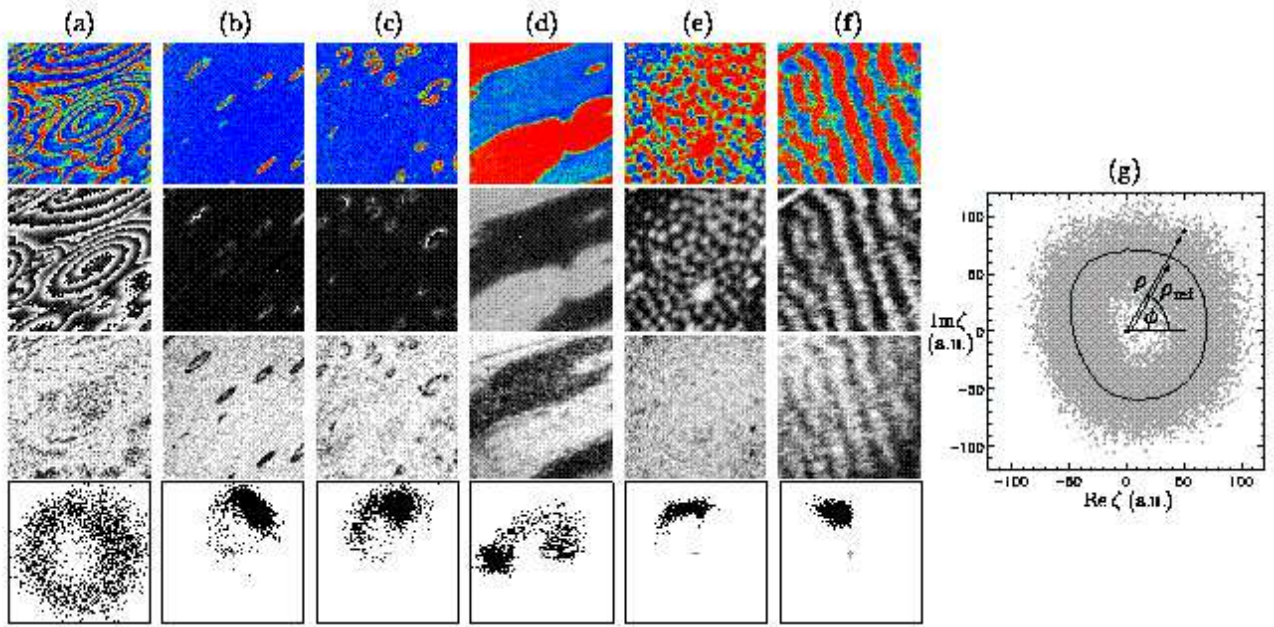


FIG. 1 (color). (a-f) PEEM images (top), distributions of phase (second row), amplitude (third row), and phase portraits (bottom) for several typical patterns observed in CO oxidation experiments. The values of temperature (K), oxygen partial pressure ( $10^{-5}$  mbar), base CO pressure  $p_0$  ( $10^{-5}$  mbar), feedback intensity  $\mu$  ( $10^{-5}$  mbar) and delay time  $\tau$  (s) are, respectively: (a) 548, 40.0, 12.3, 0, 0; (b) 540, 40.0, 13.1, 1.7, 0.7; (c) 537, 40.0, 11.4, 3.0, 0.7; (d) 500, 10.0, 3.1, 0.6, 0.8; (e) 535, 40.0, 12.2, 4.0, 0.6; and (f) 505, 10.0, 3.3, 1.6, 0.8. The side length of images is (a,b)  $360 \mu\text{m}$ , (c,d)  $330 \mu\text{m}$ , (e)  $210 \mu\text{m}$ , and (f)  $270 \mu\text{m}$ . (g) Illustration of the transformation to the amplitude  $R = \rho/\rho_{\text{ref}}(\phi)$  and phase  $\phi = \arg \zeta$  of local oscillations; the reference orbit is indicated.

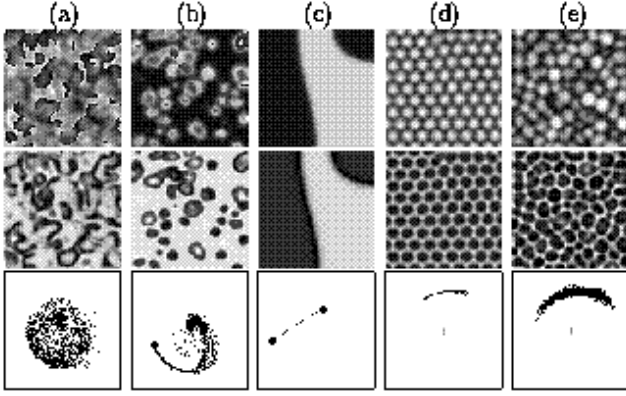


FIG. 2. Distributions of phase (top), amplitude (middle row), and phase portraits (bottom) for several typical simulated patterns. In the phase portraits (b) and (c), bold dots have been added to indicate the uniform states. The model parameters are  $k_1 = 3.14 \times 10^5 \text{ s}^{-1} \text{ mbar}^{-1}$ ,  $k_2 = 10.21 \text{ s}^{-1}$ ,  $k_3 = 283.8 \text{ s}^{-1}$ ,  $k_4 = 5.86 \text{ s}^{-1} \text{ mbar}^{-1}$ ,  $k_5 = 1.61 \text{ s}^{-1}$ ,  $s_{\text{CO}} = 1.0$ ,  $s_{\text{O}_2 \times 1} = 0.6$ ,  $s_{\text{O}_2 \times 2} = 0.4$ ,  $u_0 = 0.35$ ,  $\delta u = 0.05$ ,  $D = 40 \mu\text{m}^2 \text{ s}^{-1}$ ,  $p_{\text{O}_2} = 13.0 \times 10^{-5} \text{ mbar}$ ,  $p_0 = 4.81 \times 10^{-5} \text{ mbar}$ ,  $u_{\text{ref}} = 0.3358$ . The values of  $\mu$  ( $10^{-5} \text{ mbar}$ ) and  $\tau$  (s) are: (a) 0, 0; (b) 0.27, 0.8; (c) 0.40, 0.4; (d) 0.09, 0.3; and (e) 0.06, 0.3. The side length is (a, c-e)  $400 \mu\text{m}$  and (b)  $600 \mu\text{m}$ .